

Effect of Temperature, Pressure, and Type of Gas Injected on the Formation and Decay of Mineral Oil-Based Foams

Erich T. Tiuman, Fabrício S. da Silva, Rigoberto E. M. Morales, and Moisés A. Marcelino Neto*

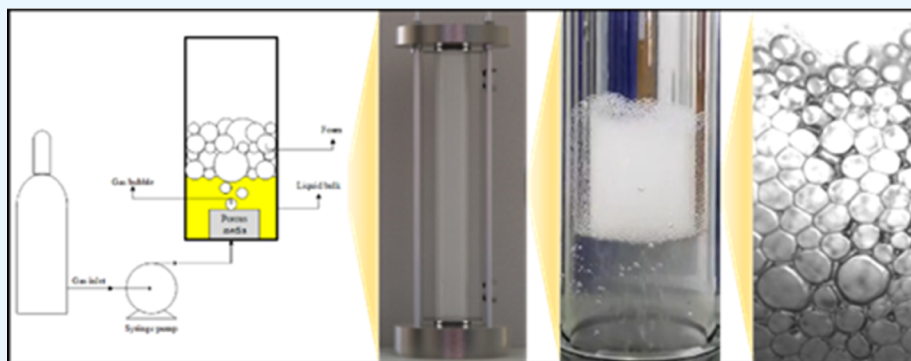
Cite This: *ACS Omega* 2023, 8, 40321–40340

Read Online

ACCESS |

Metrics & More

Article Recommendations



ABSTRACT: In three-phase gravity separators used in gas and oil production, foaming can occur by either depressurization or injection of gas in the equipment. This formed foam can be harmful, causing various problems such as liquid carry-over, gas carry-under, decreased capacity, and difficulty in level measurement. The mechanism of foam formation by gas injection in separators motivated the present study. Thus, this work proposes the analysis of the influence of certain physical–chemical parameters such as temperature (20–40 °C), pressure (1–10 bar), and types of gases (nitrogen and methane) on the formation of the column and stability of the foam formed, in ISO14 mineral oil + sodium laureth sulfate + water, through gas injection in separator conditions. To carry out this analysis, an experimental apparatus was designed and assembled consisting of a transparent foam formation cell of 0.5 m height and 5 cm internal diameter. Parameters such as foamability, foaminess, and the collapse curve were also evaluated to characterize the foam formed. In addition, simplified models of foam formation and decay by gas injection were proposed based on models already available in the literature, which were validated with the experimentally obtained results. The experimental results showed good agreement when compared to the literature, referring to the behavior of temperature (higher temperature, lower stability), pressure (higher pressure, higher stability), and type of injected gas (dependency on solubility). In addition, maximum errors of 26% (in height) and 11% (decay phase) were obtained for the formation and decay models, respectively.

1. INTRODUCTION

Foams are dispersed systems of small gas bubbles in a continuous liquid or solid phase, which may be stabilized by surfactants.^{1,2} These systems can be found in many day-to-day situations, from solutions used for cleansing to fire extinguishers. However, there are unwanted foams, such as the ones that may form during primary petroleum separation process.^{3–5}

In the oil industry, foams can be harmful to some production process, for example, during the separation step.^{4–6} In this step, foams can be formed at the three-phase gravity separators's inlet due to the pressure drop, forming gas bubbles that will consequently distend the gas–liquid interface causing the formation of these structures.^{3,4} However, according to the patent developed by Monteiro and Silva,⁷ foams can also be formed in the separator due to gas and water injected through the lower portion of the equipment, mechanism used in order to improve the separation of a three fluid phase mixture. The

formation of those structures can cause several problems in petroleum gravitational separators, such as the decrease of its capacity due to the increase in the residence time required for complete separation and due to the large volume occupied by the foams.^{3–5,8} In addition, foaming contributes to incorrect measurement of the level of the separator interfaces, another very common problem. Problems such as oil carry-over in the gas line can also occur, which can cause the contamination of this line, besides hydrolock in the gas compressors, or even gas

Received: June 26, 2023

Accepted: September 18, 2023

Published: October 16, 2023



carry-under in the oil line, consequently causing cavitation in the pump's intake line.^{3,5,6,8,9}

In the literature, few studies addressing the issue of foam formation in separators have been found. To this day, only Shaban's work⁶ deals specifically with foaming in life-size separators. Nonetheless, there are other works that deal with foam formation in simpler geometries whose motivation is to simulate the formation of foams in separators.^{3–5,8–13} These works showed the influence of defoamers or paraffins, asphaltenes, and resins on the formation and decay of foams. However, properties such as temperature, pressure, and the type of gas injected are also important in the formation and decay of foams. Thus, investigating the effect of these properties, under separator conditions and through this new mechanism of foam formation in this equipment is essential to understanding the behavior of such structures.

Some authors evaluated the influence of physicochemical parameters on foam formation and decay. Regardless of the material and method used for the formation and decay of the foam, some results are common to these structures and indicate how they behave when such parameters change. Regarding the temperature, the literature shows that an increase in this parameter generates, in most cases, a reduction in the viscosity, in the surface tension, or in the foam stability.^{1,14–25} Regarding the pressure, two different behaviors can be observed. The first behavior is that stability increases with the increase in pressure.^{23,25} In addition, some other authors confirm that stability behaves differently with an increase in pressure, as this also depends on the type of injected gas.^{18,24} Regarding the influence of the gas type on the formation and decay of foams, it is noticed that several authors share the same conclusions. There is the influence of the gas solubility, whose rate will change the foam formation and decay properties according to its increase or decrease.^{26–29}

In addition to the analysis of foam formation and decay parameters, a simplified mathematical modeling of formation and decay is presented separately. Some authors in the literature such as Bikerman,³⁰ Pilon et al.³¹ and Pilon et al.³² modeled the foaming problem, while Sita Ram Sarma et al.,³³ Narsimhan,³⁴ Dedhia et al.,³⁵ and Fortkamp and Barbosa¹⁷ studied the foam decay model.

The contribution of this work is to address the issue of the influence of physicochemical parameters on the formation and decay of foams composed mainly of mineral oil. The type of foam formation mechanism (gas injection) investigated in this work, which is closely linked to the Monteiro and Silva⁷ patent, differentiates it from other foam formation works applied to the petroleum industry. Additionally, the study investigates how certain physical factors, namely, temperature, pressure, and the composition of injected gas, influence the formation of foams primarily composed of mineral oil. To the authors' knowledge, the combined effects of these parameters have not been investigated for foams formed by mineral oil in a scenario for primary separators and foams formed by gas injection in oil production. However, given the innovative technology of this patent, the approach for foam generation in this study is the pneumatic method. As a result, one of the challenges faced is the increased complexity involved in creating and analyzing foams. This complexity arises due to the inherently less predictable nature of the foam generation mechanism when compared with the depressurization-induced mechanism. Nevertheless, the experimental setup specially designed for this research enables an evaluation of all of the specified parameters in the study.

Furthermore, although the present work uses a model oil, the intention is to evaluate the impact of physical parameters on foams formed by gas injection under gravitational separator conditions. Besides that, two simplified mathematical models will also be presented for both foam formation and decay.

2. MATERIALS AND METHODS

2.1. Test Bench. First, for the formation of the foam structure, the pneumatic method, also known as the dispersion method, was chosen. It consists of foaming by injecting gas through one or more holes at the bottom of the foaming cell.³

Figure 1 presents an illustration of the foaming method by dispersion. In this method, the foam is formed by injecting gas at

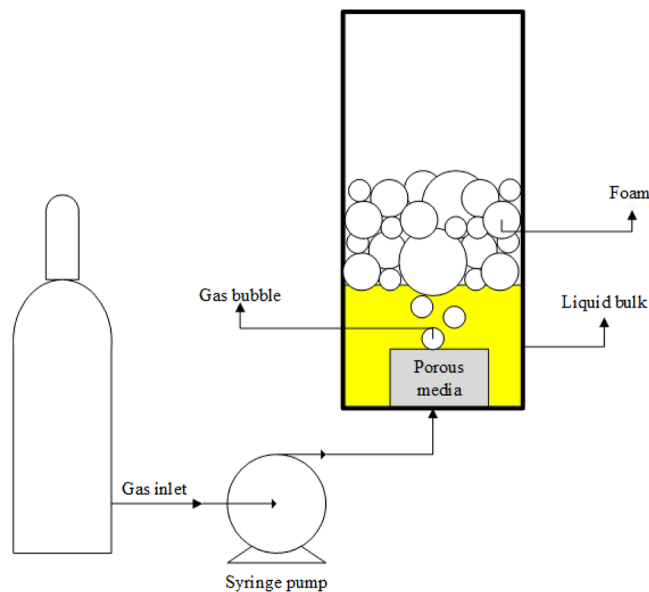


Figure 1. Dispersion method.

the bottom of the cell. This gas is fed into the cell through a pump and is inflated through a porous medium positioned at the bottom of the liquid bulk. Thus, gas bubbles are injected into the system, which will later distend the liquid–gas interface, consequently forming a foam column.

Figure 2 illustrates a schematic of the apparatus designed for foaming using the dispersion method. The gas cylinder (1) has two main functions: to pressurize the foam cell (8) and to inject gas, in a flow rate of 50 mL/min, at the bottom of the porous media (10 μm porosity) in order to create the foam column for the assessment. Starting from the gas cylinder (1), there are two lines. The first line has the sole function of pressurizing the cell (8) to the set-point pressure so that the test can start. The second line plays a fundamental role in the experiment since it will determine the foam formation mode. For having a steady and stable gas injection, it was necessary to use two syringe pumps in parallel (4) connected through a pneumatic module that controlled the communication between these equipment. With the gas flow under control, the next step is to flow this gas through the cell (8) after flowing it through a porous media that will start the process of formation of gas bubbles that distends the liquid–gas interface so that the foam forms as intended. This foam was formed inside a cell (8) composed of stainless-steel flanges connected by a 500 mm long acrylic tube with 50 mm inner diameter, as shown in Figure 3. This length was determined in such a way that the foam has enough space to

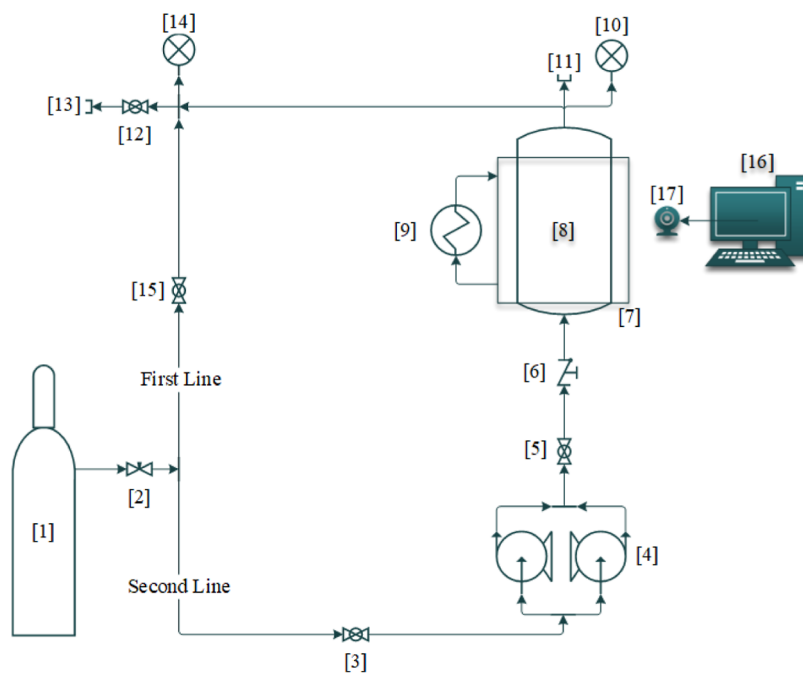


Figure 2. Schematic test loop composed by (1) gas cylinder, (2) needle valve, (3) sphere valve, (4) 2× syringe pumps, (5) sphere valve, (6) check valve, (7) temperature control reservoir, (8) foaming cell, (9) thermostatic bath, (10) pressure transducer, (11) cap, (12) sphere valve, (13) quick connector, (14) back pressure, (15) sphere valve, (16) computer, and (17) cam.

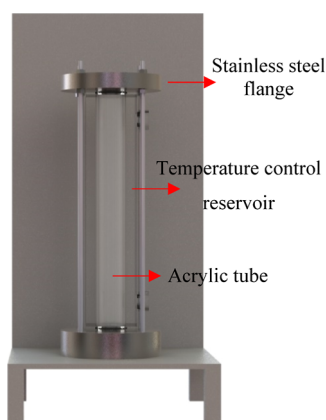


Figure 3. Foaming cell.

grow without any physical barrier blocking this growth. In the upper flange, the cell is instrumented with a pressure transducer (10) that measures its internal pressure. The apparatus also counts on a service line (11) to inject the oil to be tested inside the test cell.

Additionally, the experimental apparatus also includes a thermal bath (9) to control the temperature of the foaming cell (8), which is inserted in a transparent tank (7). A camera (17) connected to a computer (16) was used to capture the images. Finally, a high-speed camera was used to capture images relative to the physical phenomena of foam formation and decay.

2.2. Fluid Selection. Initially, examinations were conducted exclusively using ISO14 mineral oil (CAS number: 8042-47-5 from Sigma-Aldrich), with low viscosity (14.2–17.0 cst at 40 °C) and density (0.838–0.854 g/cm³ at 25 °C) that closely resemble those of the Brazilian oil fields. Additionally, ISO14 is translucent, facilitating the observation of foam growth and decay during experimental trials. However, foam formation was not verified with this pure oil or the tested gases. Thus, the use of

a foaming additive (sodium lauryl ether sulfate, anionic surfactant diluted in water) became necessary. There are several other studies that used water as a diluting agent for the foaming additive.^{36–40} Therefore, all tests were performed with 50 mL of ISO 14 mineral oil plus 2 mL of sodium lauryl ether sulfate diluted in 5 mL of water.

Regarding the gases used, they were chosen based on conventional oil fields found in Brazil. The main hydrocarbon in natural gas is methane, and nitrogen can be considered a contaminant. Therefore, the use of these gases for evaluating the results was essential.

2.3. Test Grid. The test grid, Table 1, was conceived in order to evaluate the desired parameters, such as the influence of

Table 1. Test Grid

	nitrogen			methane			
	T	P	gas	T	P	gas	
	Temperature						
P1	20 °C	1 bar	N ₂	P9	20 °C	1 bar	CH ₄
P2	25 °C	1 bar	N ₂	P10	25 °C	1 bar	CH ₄
P3	30 °C	1 bar	N ₂	P11	30 °C	1 bar	CH ₄
P4	35 °C	1 bar	N ₂	P12	35 °C	1 bar	CH ₄
P5	40 °C	1 bar	N ₂	P13	40 °C	1 bar	CH ₄
	Pressure						
P6	20 °C	1 bar	N ₂	P14	20 °C	1 bar	CH ₄
P7	20 °C	5 bar	N ₂	P15	20 °C	5 bar	CH ₄
P8	20 °C	10 bar	N ₂	P16	20 °C	10 bar	CH ₄

pressure, temperature, and type of gas injected. The tests were compared with those carried out under other conditions, so that the influence of such parameters on the foamability and stability of the foam formed could be verified.

Table 1 shows all 16 experimental points that were tested. This table is divided into two main columns where the influence of the gas type is evaluated. This is done by repeating all

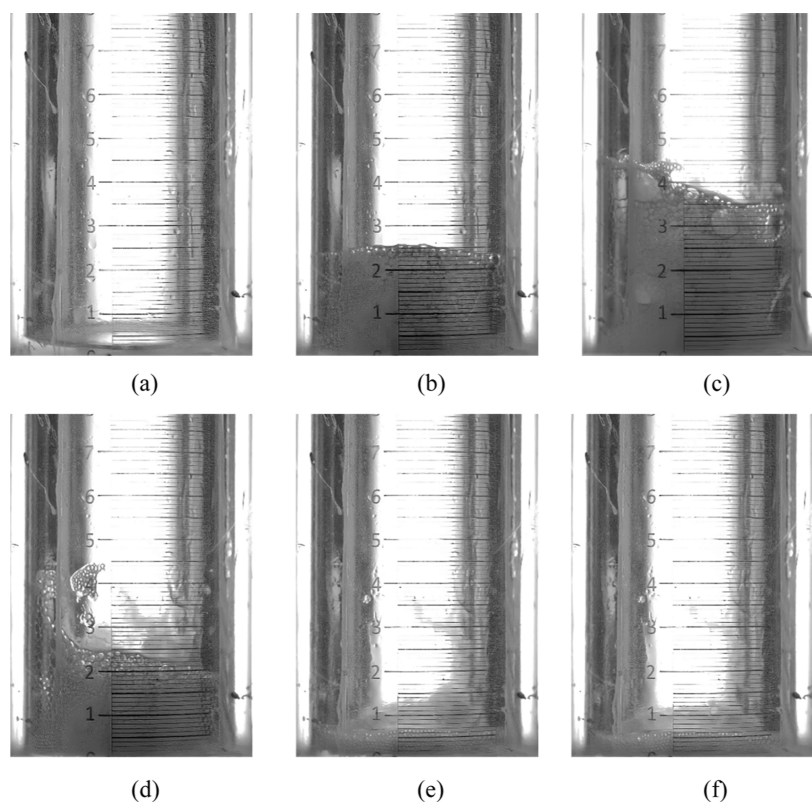


Figure 4. Illustration of the test carried out for P5. (a) $t = 0$ s, (b) $t = 260$ s, (c) $t = 530$ s, (d) $t = 620$ s, (e) $t = 1000$ s, and (f) $t = 1270$ s.

experimental points for both gases, so that the influence of such parameters can be compared. Furthermore, the Table is divided into two main parts. The first one, from points P1 to P5 and P9 to P13, aims at determining the influence of temperature since all parameters but the temperature are kept constant. Likewise, points P6–P8 and P14–P16 aim at determining the influence of pressure on foam formation and stability, as only the pressure varies in these cases and temperatures of 20 °C were chosen, as this temperature allowed a greater mechanical resistance of the rig used for the tests. Yet, points with higher temperatures might have been chosen to increase the foam decay rate.

The experimental points herein presented were chosen to fill an information gap present in the literature. This gap is related to the formation and decay of mineral oil-based foams regarding the evaluation of temperature, pressure, and type of injected gas influence. In addition, because this is a work motivated by the formation of foam in oil industry separators, the temperature and pressure measurement ranges were chosen while field parameters were taken into account and the physical limitations of the experimental rig. Also, methane gas was chosen as a model since it is the most common gas found in the natural gas.

2.4. Experimental Procedure. Before starting the experiments, it was necessary to inject the mixture oil [50 mL] + sodium lauryl ether sulfate [2 mL] + water [5 mL] through the injection line at the top of the test cell, but for the mixture to be homogeneous, an initial agitation process was necessary during 5 min by means of a magnetic agitator. The cell was then pressurized with the test gas until the pressure of the interest was reached. After this, the gas–liquid mixture in the cell requires some time to stabilize. This time must be long enough for the gas to solubilize in the liquid to be tested and for the entire system to reach the equilibrium. When this occurs, the thermal bath must already be set at the desired temperature, and the system is

expected to reach thermal equilibrium. At this moment, the image acquisition must start. It will allow verification of the height of the foam column formed, as well as the decay time after the gas injection is stopped. The back-pressure valve must be set to the pressure of interest to guarantee a stable pressure during the experiment. Thus, the role of this equipment is to regulate the pressure whenever it exceeds the previously set pressure. With all of these parameters adjusted, gas injection must occur, causing the formation of the desired foam column. For this purpose, the required flow rate in the syringe pumps must be set to 50 mL/min. Gas injection must occur until the height of the foam column becomes stable. From this moment onward, the foamability (the ratio between the formed foam column and the initial liquid volume) of the fluid can be measured. Thus, the gas injection must be shut down, and the time count for the complete decay of the foam must be started. With the given time and the intermediate foam volume measurements, a decay curve can be plotted whose collapse slope (the inclination of the decay stage) will be analyzed to determine the stability of the foam formed. To obtain the height points (H) that generate the aforementioned graphs, a graduated ruler coupled to the foaming cell was used. Each 10 s, the camera acquired an image that recorded the height of the foam layer during the execution of the experiment. This way, the formation and decay graphs can all be all plotted.

2.5. Image Analysis. Images obtained experimentally were used to obtain the graphs presented in the next subsections. With these graphs, the height of the foam column at a particular time could be evaluated. The following sequence of images illustrates the test performed at point P5.

The images illustrated by Figure 4 were obtained by repeating the experimental point P5 using a high-speed camera. This was done with the sole objective of visualizing some typical

phenomena during foam formation and decay. The images used for the construction of the foam column graphics were taken with a GoPro HERO5 Black camera. However, because of the quality of the images obtained, the images from the high-speed camera were used to illustrate the details. Figure 4a–c is related to the injection and subsequent foam formation at different time points. Figure 4d–f is related to instants of decay time of the formed foam.

2.6. Mathematical Modeling of Foam Formation. In this section, an approach based on Pilon et al.³² is presented. These researchers developed a mathematical model for the prediction of foam layer thicknesses as a function of time for foams formed by gas injection (pneumatic test).

The model is based on the following assumptions: (1) the problem is one-dimensional and transient; (2) wall effects are negligible; (3) the foam is isothermal; and (4) during transient formation, there will be no bursting on the foam surface.

Figure 5 illustrates the schematic diagram of the problem and the geometry.

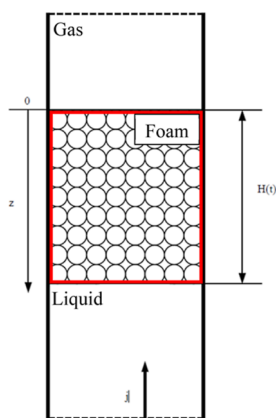


Figure 5. Scheme of foam generation through gas injection. Source: adapted from Pilon et al.³²

Figure 5 shows a circular compartment for the formation of the foam column with a cross-sectional area equal to A . At time $t = 0$, gas is injected into the system through the lower part of the compartment at a constant superficial velocity j , which is faster than the minimum speed required for foaming, also known as j_m . $H(t)$ is the height of the foam column at any instant of time t . The origin of the chosen coordinate system is located at the top of the foam, and its growth direction is the z axis. The control volume is delimited by the red rectangle and indicates the foamy volume formed in the compartment.

The foam will grow until it reaches a steady state. At this point, the height will remain stable until the gas injection is stopped, and the height in steady state is called H_∞ . This happens at a time called τ . The derivation process leading to the (1) can be found in the Appendix Section.

$$H(t) = \frac{jt}{\phi} \text{ if } t \leq \tau \quad (1)$$

This is the simplest expression one can find to calculate the foam layer height as a function of the time for foams formed through gas injection.

Yet it is still necessary to calculate the critical time, that is, the moment when the foams stop growing and reach a plateau. This should be done from the following correlation described by Pilon et al.³²

$$\tau = \frac{\bar{\phi} H_\infty}{j} \quad (2)$$

where τ is the critical time, H_∞ is the plateau foam layer, and j is the superficial gas velocity.

However, to define H_∞ another correlation presented by Pilon and Viskanta⁴¹ must be used

$$H_\infty = 2905 \frac{\sigma [\mu_1(j_g - j_m)]^{0.8}}{r^{2.6} (\rho_1 g)^{1.8}} \quad (3)$$

where H_∞ is the steady-state height of the foam, σ is the surface tension of the fluid, r is the bubble radius estimated through foam column images and a code developed in MATLAB to obtain the average bubble radius of the structure, μ_1 is the liquid viscosity, j_g is the superficial gas velocity, j_m is the superficial gas velocity for onset of foaming, ρ_1 is the liquid density, and g is the gravity.

Estimating the minimum superficial velocity necessary to form foam is a quite complicated task, but the correlation presented by Pilon and Viskanta⁴¹ can be used in this case

$$j_m = \nu_\infty f(r^*) \text{FiM} (1 - \text{FiM})^{n-1} \quad (4)$$

where ν_∞ is the bubble terminal speed, $f(r^*)$ is a function of dimensionless radius r^* and the flow pattern, FiM is the maximum void fraction for onset of foaming, and n is a constant experimentally determined.

All the information necessary in order to calculate the parameter j_m are described in Pilon and Viskanta.⁴¹ The only difference is the variable FiM ; in this work, it was used to calibrate the model using the experimental results of maximum foam height in steady-state. Unlike Pilon and Viskanta,⁴¹ where the variable j_m was measured experimentally, in this study, this variable was calculated. To accomplish this, the variable FiM was determined through several tests to fit the model results in comparison to the experimental data. Additionally, a linear regression was performed between this variable and temperature to provide a physical interpretation of FiM . The use of FiM in calibrating the model produced satisfactory results, and further information on this variable can be found in Section 3.3.

2.7. Mathematical Modeling of Foam Decay. The drainage model developed in this section is based on the model presented by Fortkamp and Barbosa,¹⁷ with some modifications. As the original model was for foams formed through the condensation method (foam formation due to depressurization), some properties such as pressure, gas solubility, specific mass of the mixture, and others vary over time. However, as the present work uses the pneumatic foaming method, it is not necessary to consider such variations of properties. Therefore, the model to be developed in this section presents some modifications.

Based on visual observations of foam decay, the drainage rate can be modeled as being directly proportional to the foam height given the following expression¹⁷

$$\dot{m}_L = m_0'' A \left[\exp\left(C_4 \frac{t}{\tau}\right) \right] \quad (5)$$

where \dot{m}_L is the foam drainage rate, m_0'' is the proportionality term, A is the cross-sectional area, C_4 is an empirical constant, t is the time, and τ is the characteristic time.

The proportionality term can still be written as follows

$$m_0'' = C_3 \bar{\rho} \sqrt{gH_f} \quad (6)$$

where C_3 is an empirical constant (equivalent to a discharge or flow coefficient, that is, related to the drainage velocity, the velocity within the liquid flows through the Plateau borders⁴² of the foam), $\bar{\rho}$ is the average density of the foam, g is the gravity, and H_f is the foam height.

The variable τ is used to make the time in the exponential function dimensionless. This variable can be defined as the ratio between the characteristic height and the characteristic velocity that will be defined soon

$$\tau = \frac{H_c}{U_D} \quad (7)$$

However, the characteristic height can be defined as the initial height of liquid H_L .¹⁷

To define the characteristic velocity, that is, the superficial velocity of the liquid in the Plateau borders, Fortkamp and Barbosa¹⁷ used an analogy with porous media, determining such velocity from Darcy's law for low-velocity flows. Thus, according to Kaviany⁴³

$$-\frac{dP}{dz} = \frac{\mu_1 U_D}{K} \quad (8)$$

where $\frac{dP}{dz}$ is the hydrostatic pressure gradient, μ_1 is the liquid viscosity, and K is the porous media permeability. Assuming that the foam is in mechanical equilibrium, the hydrostatic pressure gradient can be written as follows

$$\frac{dP}{dz} = -\rho g \quad (9)$$

The average density can be written as

$$\bar{\rho} = (1 - \phi)\rho_l + \phi\rho_g \quad (10)$$

where ϕ is the void fraction, ρ_l is the liquid density, and ρ_g is the gas density.

From (8)–(10), an expression for the surface velocity of the liquid in the Plateau borders can be obtained

$$U_D = \bar{\rho} g \frac{K}{\mu_l} \quad (11)$$

A correlation for the permeability of the foam is still required. Thus, the Carman–Kozeny model can be used⁴³

$$K = \frac{4(1 - \phi)^3 r^2}{180\phi^2} \quad (12)$$

3. RESULTS AND DISCUSSION

Initially, tests were carried out to validate the experimental methodology used and to verify the repeatability of the experimental procedure. After that, tests with nitrogen were conducted in order to compare the influence of the temperature and pressure on the formation and decay of foams through the gas injection method. Finally, the test grid was repeated completely for methane gas so that it was possible to evaluate the influence of the type of gas injected.

Several numerical computations were performed using MATLAB software to obtain the results through the mathematical modeling of foam formation and decay. The experimental results were used to calibrate the mathematical models.

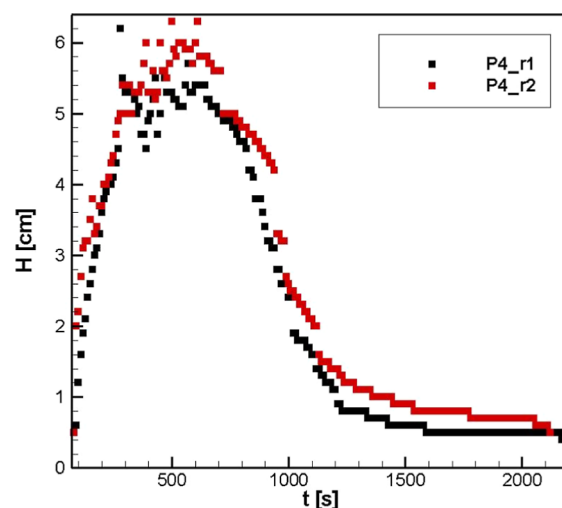


Figure 6. Experiment repeatability verification. One bar, 35 °C, injected gas: N₂, liquid mixture: 50 mL of ISO14 mineral oil + 2 mL of sodium lauryl ether sulfate + 5 mL of water.

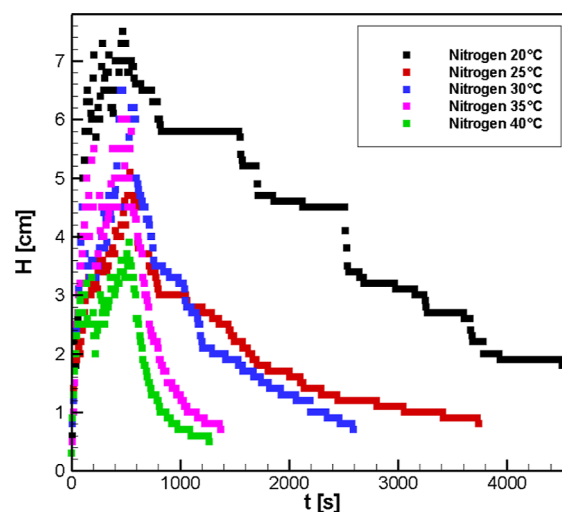


Figure 7. Experimental results for temperature influence with 1 bar of nitrogen gas.

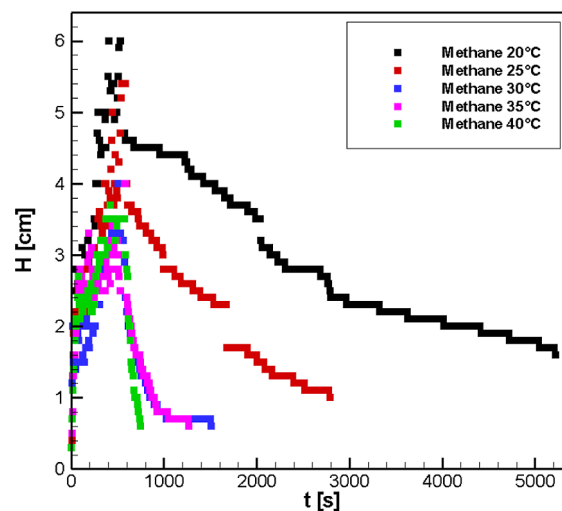


Figure 8. Experimental results for temperature influence with 1 bar of methane gas.

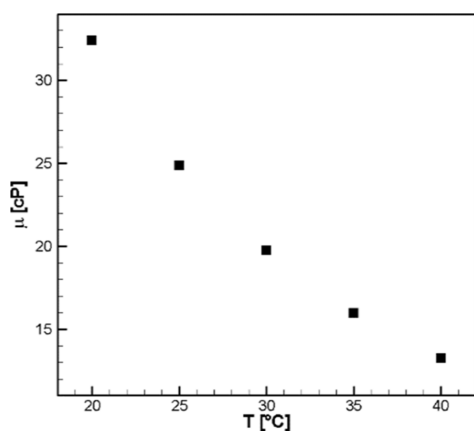


Figure 9. Experimental results for mixture viscosity (50 mL of ISO14 mineral oil +2 mL of sodium lauryl ether sulfate +5 mL of water).

Table 2. Quantitative Results for Foam Formation and Decay: Temperature

experimental point	foamability	collapse slope [cm/s]	collapse time [s]
Nitrogen			
P1	22.63	−0.0012	1990
P2	13.83	−0.0019	960
P3	17.33	−0.0044	530
P4	16.87	−0.0144	160
P5	10.57	−0.0138	160
Methane			
P9	16.77	−0.0010	2240
P10	15.03	−0.0019	810
P11	9.83	−0.0119	190
P12	9.47	−0.0090	160
P13	10.53	−0.0279	60

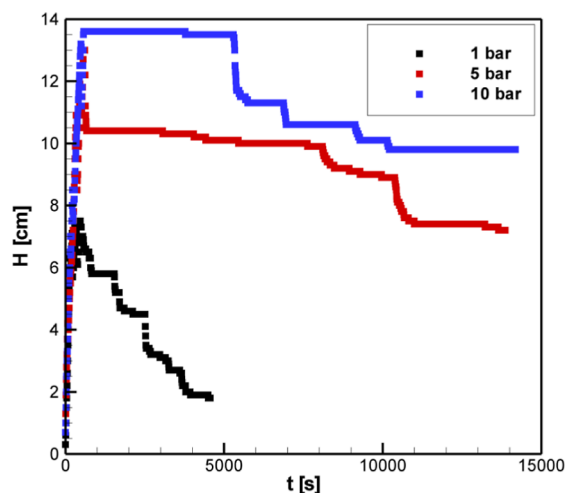


Figure 10. Experimental results for pressure influence with 20 °C nitrogen gas.

3.1. Repeatability Verification. To verify the repeatability of the experiment, two identical experimental points were performed. All parameters of pressure (1 bar), temperature (35 °C), type of injected gas (N₂), and mixture composition were kept constant (experimental point P4). To perform each test, the same cleaning procedures were performed on the experimental rig, and the mixture was performed identically and with the same agitation time to minimize any differences

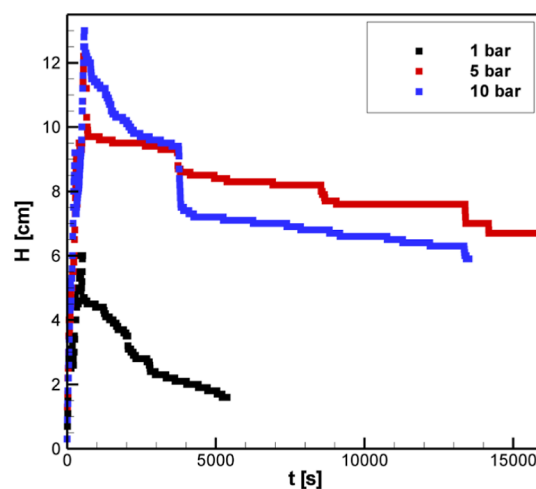


Figure 11. Experimental results for pressure influence with 20 °C methane gas.

due to the procedure. Both tests were performed with the mixture used for the entire experimental grid: 50 mL of ISO14 mineral oil +2 mL of sodium lauryl ether sulfate +5 mL of water.

Figure 6 presents the results obtained through the tests carried out for point P4. As it can be seen, the two tests showed similar results, indicating that there is repeatability in the experimental methodology used.

There are some visual differences between the foams formed when comparing P4_r1 to P4_r2, although these differences are due to the randomness of the foam formation and decay due to the physical characteristics of this structure. Thus, it is possible to perform the experiments following the suggested methodology.

3.2. Experimental Results. 3.2.1. Temperature. In order to evaluate the influence of the temperature parameter on foam formation and decay, some tests varying this parameter between 20 and 40 °C were performed. In addition, the foamability, the collapse slope, and the collapse time were calculated, allowing the evaluation of these experimental points and a future discussion on the results obtained.

Figures 7 and 8 present the experimental results obtained for the formation and decay of foams for nitrogen and methane, respectively.

Evaluating the graphs qualitatively, a very clear trend of an increasing decay rate can be observed as the temperature increases for both gases. This was an expected behavior, as some authors had previously verified.^{14–17,19,20,22,44} Although the authors cited above used different gas and liquid compositions for the formation of the foam column, many of the results can be compared with those of the present work because of the physical characteristics/properties of the foams.

This decrease in the stability of the foam column formed can be explained by some phenomena that occur in the foam structure due to an increase in temperature. However, the most common is due to a decrease in viscosity as a consequence of increasing temperatures. This decrease in viscosity increases the flow velocity through the Plateau borders, i.e., the liquid drainage through the bubbles become easier, and consequently the liquid film between the bubbles tends to become thinner quicker, which ends up contributing to phenomena such as bursting (rupture of bubble) and bubble coalescence (this phenomenon occurs when the interstitial film connecting two or more bubbles is disrupted due to its inherent fragility, leading to

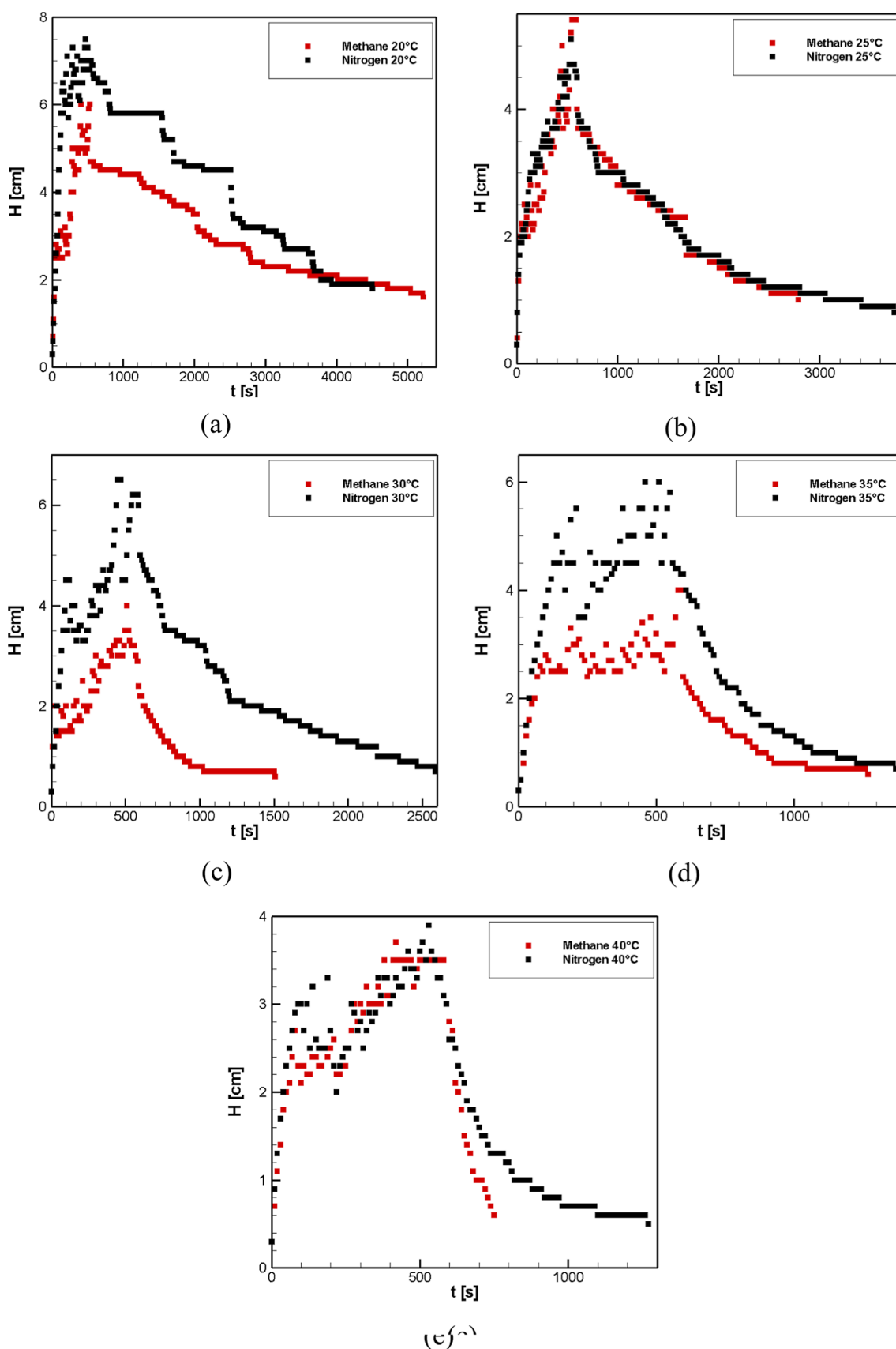


Figure 12. Experimental results for type of gas injected evaluated for (a) $T = 20^\circ\text{C}$, (b) $T = 25^\circ\text{C}$, (c) $T = 30^\circ\text{C}$, (d) $T = 35^\circ\text{C}$, and (e) $T = 40^\circ\text{C}$.

a consequent reduction in the overall bubble population⁴⁵). These phenomena are directly related to foam collapse, so there

is an increase in the decay rate, that is, a decrease in foam stability. To corroborate the analysis presented here, the

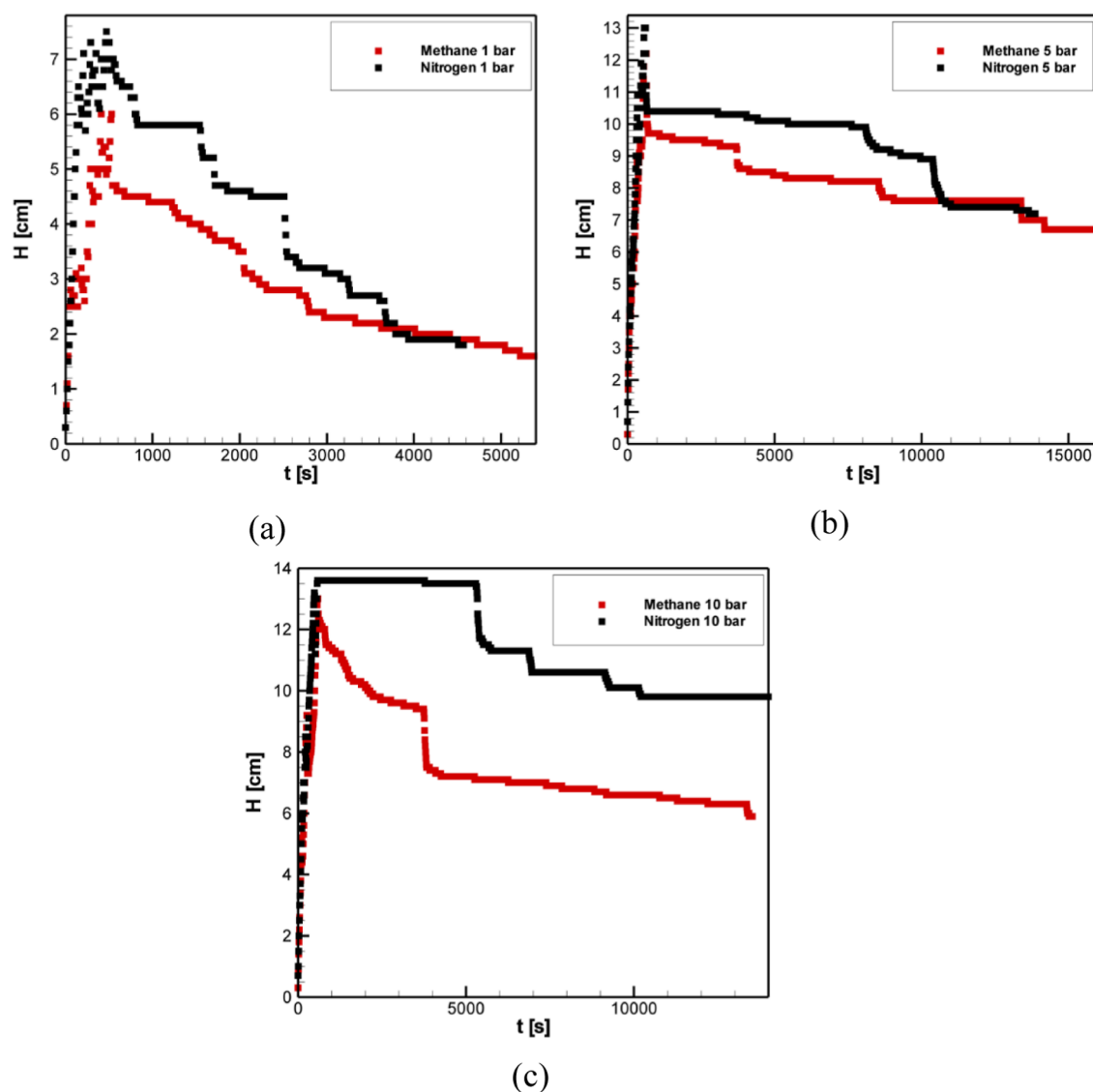


Figure 13. Experimental results for type of gas injected for (a) $P = 1$ bar, (b) $P = 5$ bar, and (c) $P = 10$ bar.

viscosity of the mixture was evaluated by using a Brookfield LVDV-II+P viscometer. The results obtained are presented in Figure 9.

It is also possible to see through Figures 7 and 8 that there are some “steps” during the foam decay phase, especially at lower temperatures. These “steps” occur because of the stabilization of large bubbles in the structure. The larger the bubbles, the greater the step presented because the foam volume drops considerably when one of these large bubbles collapses.

To quantitatively evaluate the results, the parameters of foamability, collapse slope, and foam collapse time were calculated. These data are presented in Table 2.

Two main points can be evaluated in Table 2. First, there is a trend toward reduced foamability, for both nitrogen and methane, except points P2 and P13. This reduction in foamability due to the increase in temperature can also be explained by the increase in the flow velocity through the Plateau borders. This is because the growth of a foam column is a competition between the phenomena that make that structure grow (e.g., creaming), forces that act on foam growth (such as buoyancy), those that cause the foam to decay (e.g., bursting, bubble coalescence, and drainage velocity), and the gravitational

force. With an increase in temperature and, consequently, an increase in drainage velocity, the forces related to the decay of the foam end up prevailing. This way, the foam ends up not growing as much as it would at lower temperatures, which is in agreement with what was observed by Fortkamp and Barbosa.¹⁷

Furthermore, it can be observed that both the collapse slope and the collapse time tend to increase at higher temperatures. This is in line with what was qualitatively observed through the graphs, that is, the higher the temperature, the lower the foam stability, a fact that was also observed by other authors in the literature as Abd Rahim et al.¹⁴ and Jackman et al.²⁰

3.2.2. Pressure. The influence of the pressure through pneumatic foam formation and decay tests was also evaluated. In this case, six tests were performed for both gases and pressures ranging between 1 and 10 bar. Figures 10 and 11 present the results obtained from the experiments.

According to the literature, the influence of this parameter is quite controversial because in addition to the influence of pressure in the system, the type of gas also influences the behavior of the foam during its decay.^{18,25}

For foams formed by nitrogen, a clear increase in stability can be observed with an increase in pressure. This can be explained

Table 3. Quantitative Results of Foaminess: Influence of Type of Gas Injected

experimental point	steady-state foam volume [mL]	gas rate [mL/min]	foaminess [s]
Nitrogen			
P1	139.21	50	167.05
P2	87.38	50	104.85
P3	107.99	50	129.59
P4	105.24	50	126.29
P5	68.13	50	81.76
P6	139.21	50	167.05
P7	225.02	50	270.02
P8	245.83	50	295.00
Methane			
P9	104.65	50	125.59
P10	94.44	50	113.33
P11	63.81	50	76.58
P12	61.65	50	73.98
P13	67.94	50	81.52
P14	104.65	50	125.59
P15	223.05	50	267.66
P16	226.59	50	271.90

on the grounds of pressure-related phenomena in the foam structure. Among these phenomena, the decrease in the bubble radii that form the foam can be highlighted. This decrease causes an increase in stability, as it is already known that smaller bubbles tend to have a longer life before collapsing.⁴⁶ In addition, a structure composed of smaller and more uniform bubbles tends to be more stable. This could be because some phenomena such as the Ostwald ripening, which is the smaller species gradually vanish over time, while the dissolved material is transferred to the larger species,² and bubble coalescence become less accelerated. Furthermore, this increase in stability can be linked to the decrease in the size of the Plateau's borders. Because of a decrease in the bubbles' radii presented in the structure, the Plateau borders, consequently, exhibit smaller dimensions, and thus, the flow through these channels becomes slower, generating a decrease in the decay rate of the foam, that is, a significant increase in its stability.

However, upon evaluation of the foam formed by methane, a slightly different behavior is found. An increase in stability can be observed between 1 and 5 bar, where the stability of the foam clearly increases with the increase in pressure. However, when the pressure is increased from 5 to 10 bar, a decrease in stability can be observed. A behavior similar to this one had already been observed in the literature²⁴ for CO₂ foams. This fact can be explained by an increase in the solubility of the gas with an increase in pressure. In this case, the foam would tend to decay more quickly since part of the gas present in this structure would solubilize into the liquid, causing some phenomena such as Ostwald ripening and bubble coalescence to accelerate further, thus causing a decrease in stability.

3.2.3. Type of Gas Injected. Finally, the influence of the type of gas injected on the formation and decay of foams was evaluated. To achieve this, all experimental cases were tested for both nitrogen and methane. Figures 12 and 13 present the results obtained.

As can be seen, methane foams show a strong trend to grow less and decay faster when compared to nitrogen for all cases except the 25 °C or P2 point. This can be explained on the grounds of a higher solubility of methane. This characteristic

the gas influences several phenomena responsible for foam formation and decay. First, gases with higher solubility will enhance phenomena, such as Ostwald ripening and bubble coalescence. This happens because gaseous mass transfer accelerates these processes. An increase in these phenomena will cause a decrease in the size of the foam column as there is greater competition between the forces of growth and decay of this structure. In addition, such phenomena will accelerate the foam decay process, as they will increase the size of the bubbles, causing Plateau borders to become bigger and, consequently, an acceleration of the flow velocity through these regions. Furthermore, an increase in the aforementioned phenomena will contribute to a more prominent bursting phenomenon, which will accelerate the decay of the foam formed. Such a behavior was already observed by Hartland et al.,²⁸ where gases with higher solubility tended to form smaller foam columns and accelerate the decay process; thus, the results herein presented are in agreement with those shown in the literature.

Moreover, the influence of the type of gas can be evaluated through the calculation of foaminess, which represents the amount of foam formed by the ratio of the injected gas; that is, the greater the foaminess, the more foam a certain type of gas can form using the same injection rate. The results of the foaminess calculation are shown in Table 3.

It can be seen that with the exception of points P2 and P10, the other corresponding pairs comparing nitrogen and methane, that is, P1 and P9, P3, P11, and so on, all nitrogen points have higher foaminess. This means that the quantitative results presented herein are in agreement with the graphical analysis previously performed and only reinforces the supposition that foams formed by methane tend to grow less than those formed by nitrogen gas.

3.3. Mathematical Modeling. **3.3.1. Formation.** In this section, the results obtained through the mathematical modeling based on Pilon et al.³² will be presented. This model depends on an experimentally adjusted variable called the maximum void fraction for the onset of foaming (FiM). Next, the results obtained when this variable was adjusted for each temperature will be presented, and later, the results will be presented after a linear regression of the points obtained. Figures 14 and 15 present the results for which the variable was independently adjusted.

To adjust the foam column formation curves, a linear regression was performed on the results obtained through the mathematical modeling in order to make the FiM variable temperature-dependent. Figure 16 illustrates this linear regression.

The results obtained with temperature-dependent FiM are shown in Figures 17 and 18.

It can be seen through the results herein presented that there is a small difference between the individual adjusted formation modeling results and the results adjusted through a linear regression of the maximum void fraction for the onset of foaming. This difference is illustrated in Tables 4 and 5 with the results of deviations as a function of height and time for both cases.

It can be observed that the adjustment of the FiM variable brings good results for the model when compared to the experimental data for foam height column, but the errors regarding the time required to reach the maximum height are still quite high. This originates from the simplified formulation of the mathematical modeling, and therefore some phenomena that occur during the foam formation stage, such as bursting at

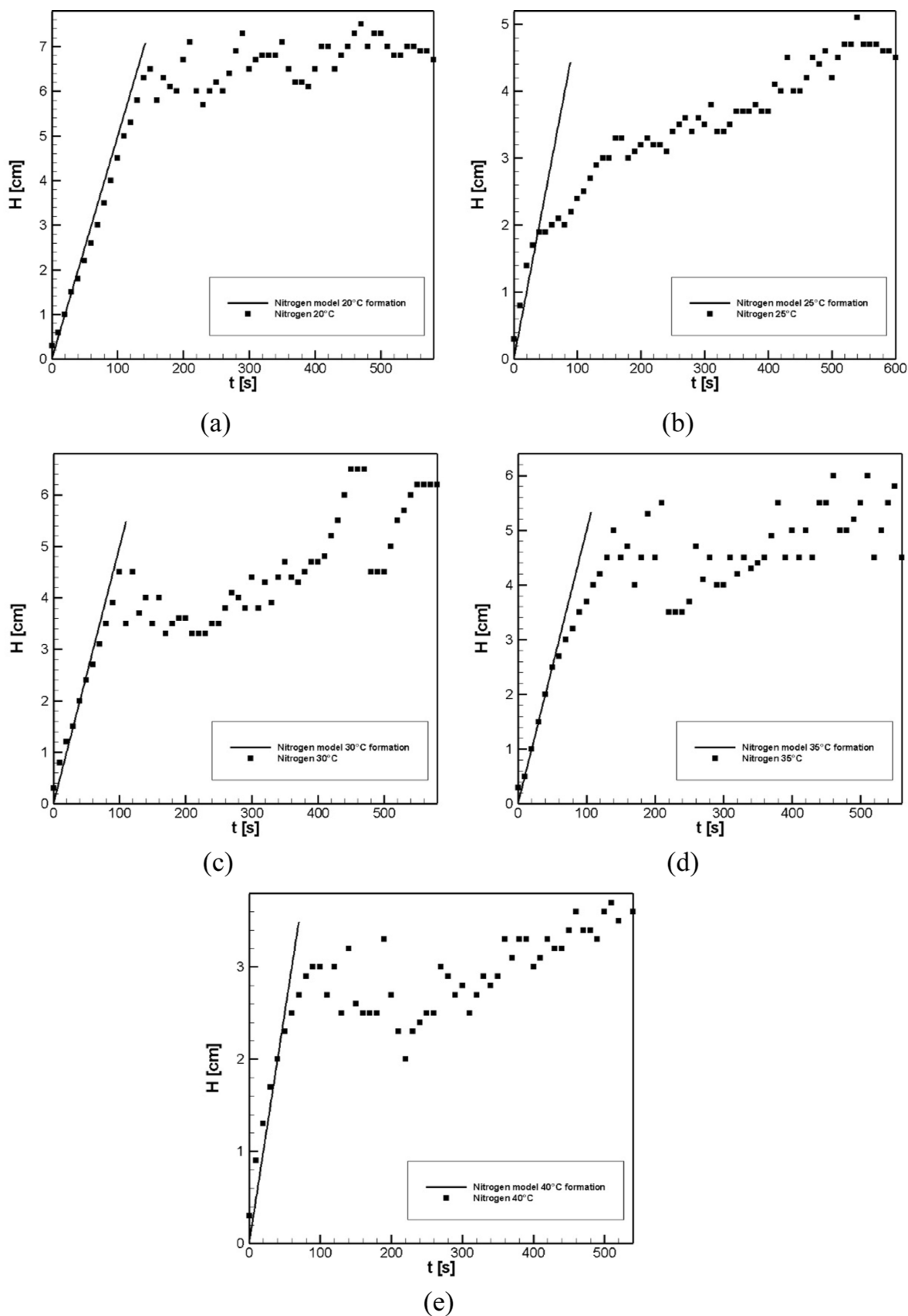


Figure 14. Formation model results for 1 bar nitrogen. (a) $T = 20\text{ }^{\circ}\text{C}$, (b) $T = 25\text{ }^{\circ}\text{C}$, (c) $T = 30\text{ }^{\circ}\text{C}$, (d) $T = 35\text{ }^{\circ}\text{C}$, and (e) $T = 40\text{ }^{\circ}\text{C}$.

the top of the column, are not taken into account, making the model reach the steady state before the experimental procedure.

In addition, the type of foam formed through the experiment is in line with the results shown in the article of Pilon et al.³² as type

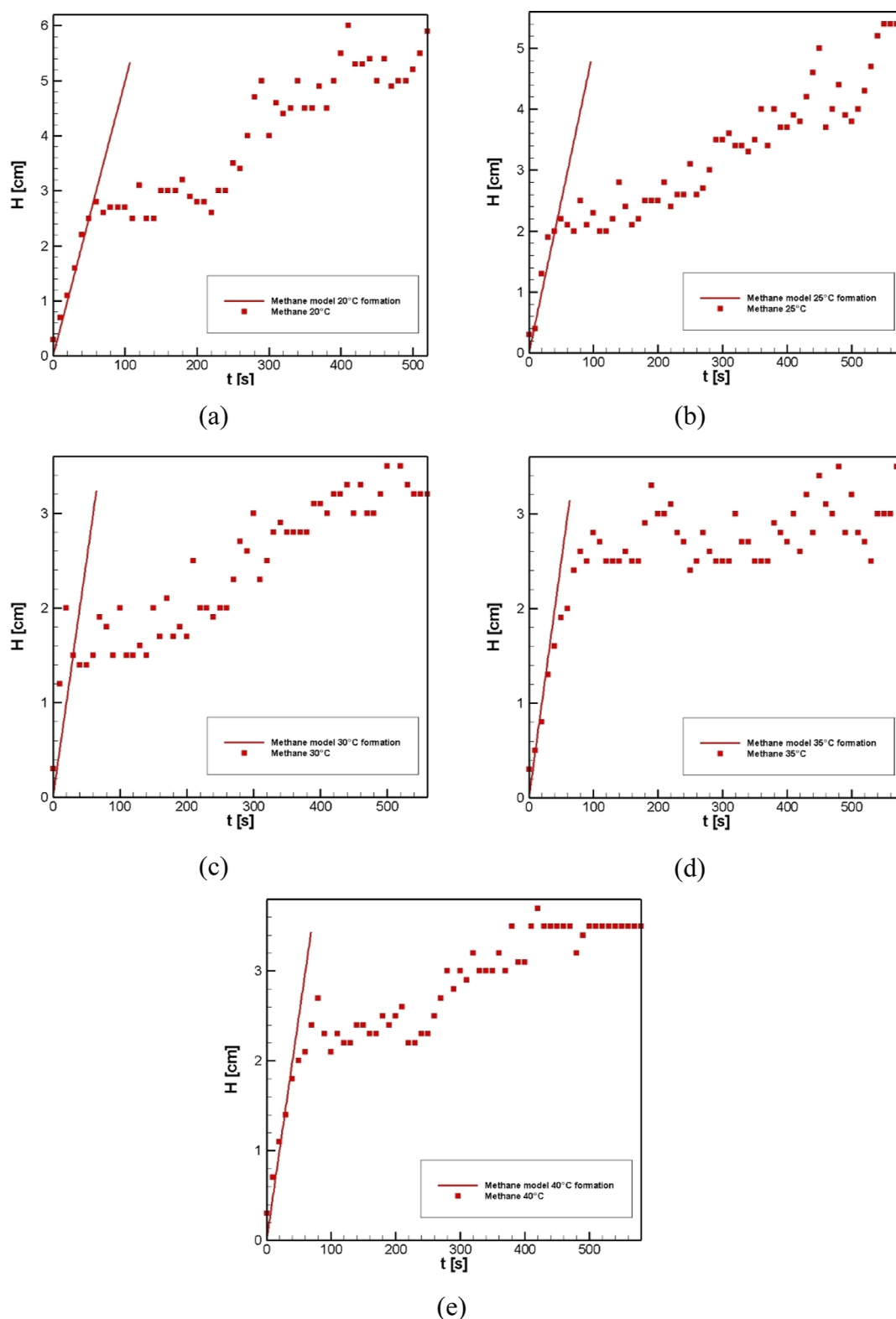


Figure 15. Formation model results for 1 bar methane: (a) $T = 20\text{ }^{\circ}\text{C}$, (b) $T = 25\text{ }^{\circ}\text{C}$, (c) $T = 30\text{ }^{\circ}\text{C}$, (d) $T = 35\text{ }^{\circ}\text{C}$, and (e) $T = 40\text{ }^{\circ}\text{C}$.

2 foam, that is, a foam that has oscillations around the total height value in steady state. As the model considers that the formation of the foam column presents a linear behavior, this is also linked to the observed time error, as also observed by Pilon et al.³² Finally, it can be pointed out that the model has a satisfactory correlation with the experimental data when observing the maximum values of foam height in steady state

as well as a good convergence with respect to the behavior of foam heights with increasing temperatures, where the model is able to capture this behavior of foam layer decrease due to viscosity reduction.

3.3.2. Decay. In this section, the results of the mathematical modeling of foam decay based on Fortkamp and Barbosa¹⁷ will be presented. Given the difference in the type of foam formed,

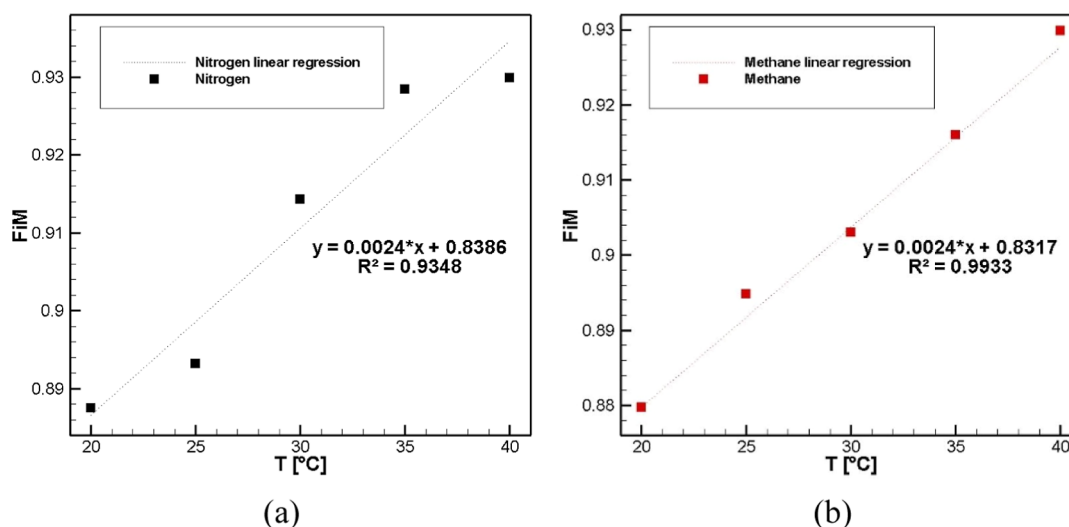


Figure 16. Linear regression results carried out for FiM parameter with temperature. (a) Nitrogen and (b) methane.

Table 4. Quantitative Results of Foam Column Formation Modeling

temperature [°C]	FiM	experimental height [cm]	model height [cm]	height deviation	experimental time [s]	model time [s]	time deviation	
Nitrogen								
P1	20	0.8875	7.1	7.083	0.095%	210	142	32%
P2	25	0.8932	4.5	4.440	0.235%	430	89	79%
P3	30	0.9143	5.5	5.487	0.235%	430	110	74%
P4	35	0.9285	5.4	5.337	0.421%	380	107	72%
P5	40	0.9299	3.5	3.492	0.627%	450	70	84%
Methane								
P9	20	0.8797	5.3	5.337	0.139%	400	107	73%
P10	25	0.8948	4.8	4.789	0.443%	540	96	82%
P11	30	0.9030	3.3	3.242	0.235%	420	65	85%
P12	35	0.9160	3.1	3.143	0.082%	190	63	67%
P13	40	0.9299	3.5	3.442	0.524%	380	69	82%

Table 5. Quantitative Results of Adjusted Foam Column Formation Modeling

temperature [°C]	FiM	experimental height [cm]	model height [cm]	height deviation	experimental time [s]	model time [s]	time deviation	
Nitrogen								
P1	20	0.8866	7.1	6.884	2.909%	210	138	34%
P2	25	0.8986	4.5	5.587	25.547%	430	112	74%
P3	30	0.9106	5.5	4.789	12.933%	430	96	78%
P4	35	0.9226	5.4	4.390	18.104%	380	88	77%
P5	40	0.9346	3.5	4.190	20.753%	450	84	81%
Methane								
P9	20	0.8797	5.3	5.337	0.139%	400	107	73%
P10	25	0.8917	4.8	4.090	14.961%	540	82	85%
P11	30	0.9037	3.3	3.392	4.369%	420	68	84%
P12	35	0.9157	3.1	3.093	1.506%	190	62	67%
P13	40	0.9277	3.5	3.093	10.615%	380	62	84%

the modeling presented by Fortkamp and Barbosa was simplified so that it could be applied to gas-injected foam.

In this model, the two coefficients C_3 and C_4 must be adjusted. However, the C_4 coefficient does not significantly influence the decay model for gas injection foams, and hence, the value presented by Fortkamp and Barbosa¹⁷ (5.0×10^{-3}) was used to obtain the results. Mathematical computations were performed for each of the experimental points in order to obtain an optimized C_3 coefficient. For each computation, the root-mean-square error (RMSE) was evaluated. The achievement of the optimized C_3 coefficient was given by the smallest error

obtained. Table 6 shows the results obtained from C_3 as well as the RMSE and normalized RMSE which is the RMSE normalized with the maximum height of foam for each case.

It can be seen that the average deviation of the normalized RMSE is 7%, indicating a good correlation between the mathematical modeling and the experimental points used. Each point has an individual C_3 coefficient as this coefficient is mainly related to the flow of liquid through the Plateau borders. Besides, the C_3 coefficient still has the function of correcting deviations from the presented model, a fact that was also observed by Fortkamp and Barbosa¹⁷. The results obtained

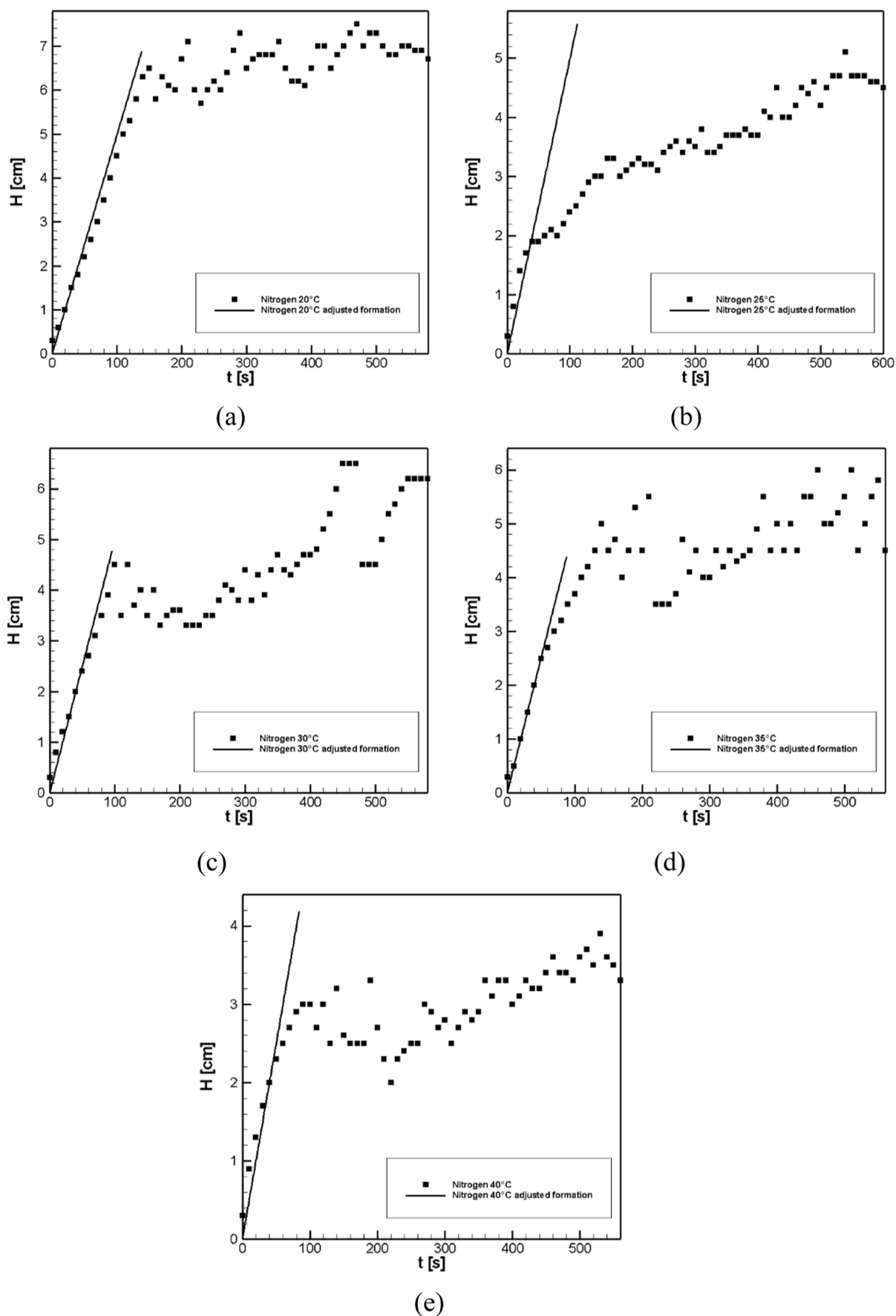


Figure 17. Adjusted formation model results for nitrogen. (a) $T = 20\text{ }^{\circ}\text{C}$, (b) $T = 25\text{ }^{\circ}\text{C}$, (c) $T = 30\text{ }^{\circ}\text{C}$, (d) $T = 35\text{ }^{\circ}\text{C}$, and (e) $T = 40\text{ }^{\circ}\text{C}$.

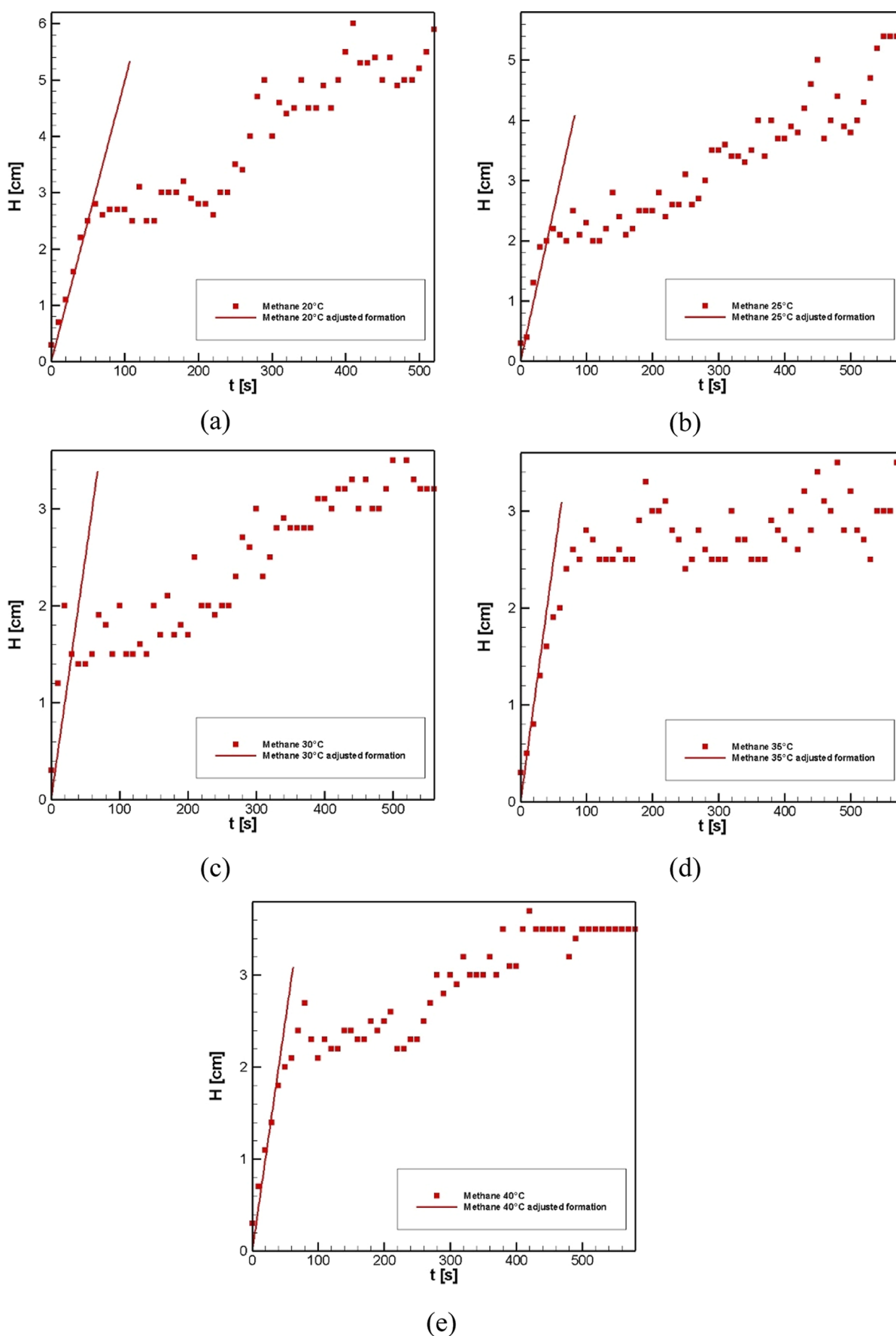


Figure 18. Adjusted formation model results for methane. (a) $T = 20\text{ }^{\circ}\text{C}$, (b) $T = 25\text{ }^{\circ}\text{C}$, (c) $T = 30\text{ }^{\circ}\text{C}$, (d) $T = 35\text{ }^{\circ}\text{C}$, and (e) $T = 40\text{ }^{\circ}\text{C}$.

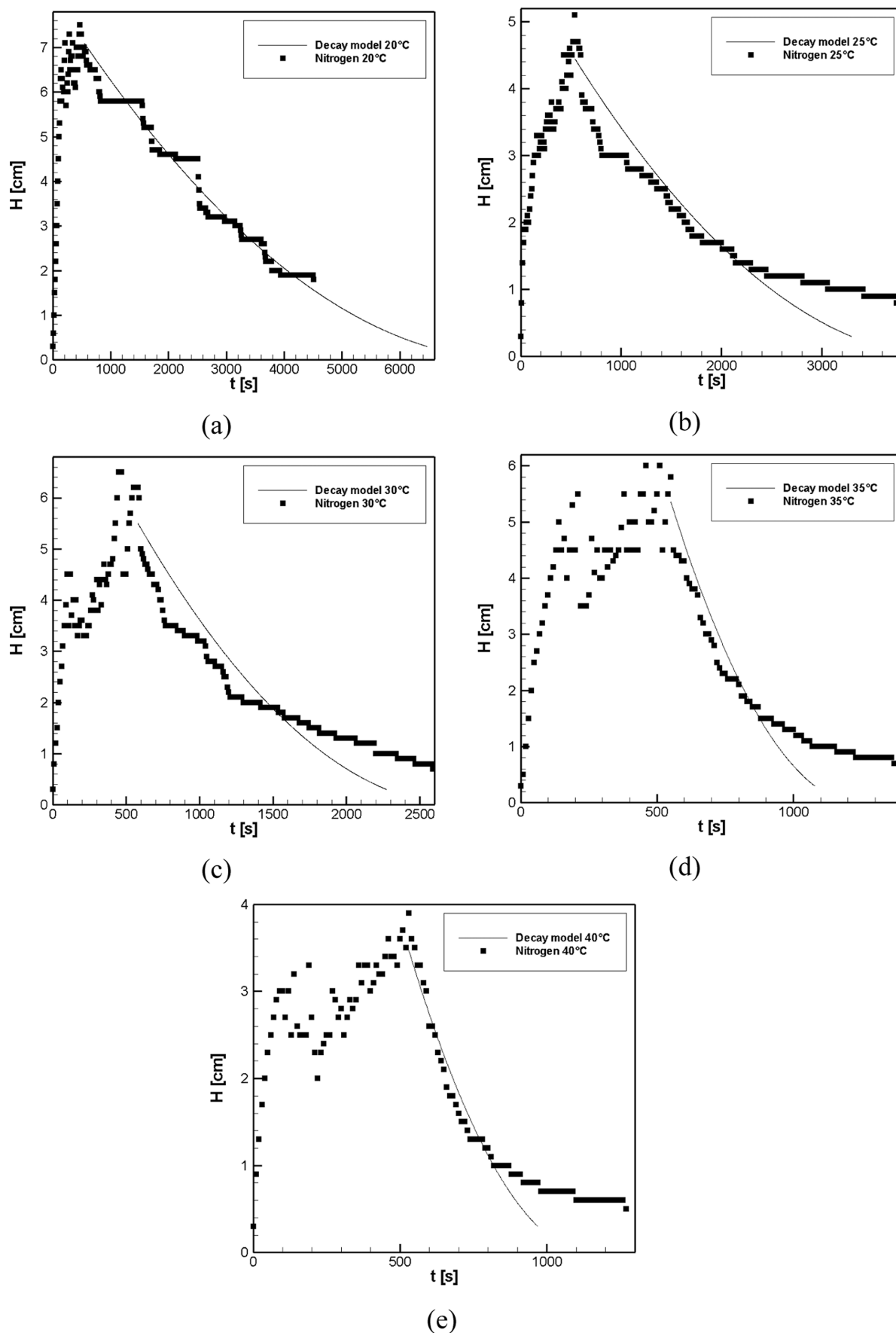


Figure 19. Decay mathematical modeling results for 1 bar nitrogen. (a) $T = 20^\circ\text{C}$, (b) $T = 25^\circ\text{C}$, (c) $T = 30^\circ\text{C}$, (d) $T = 35^\circ\text{C}$, and (e) $T = 40^\circ\text{C}$.

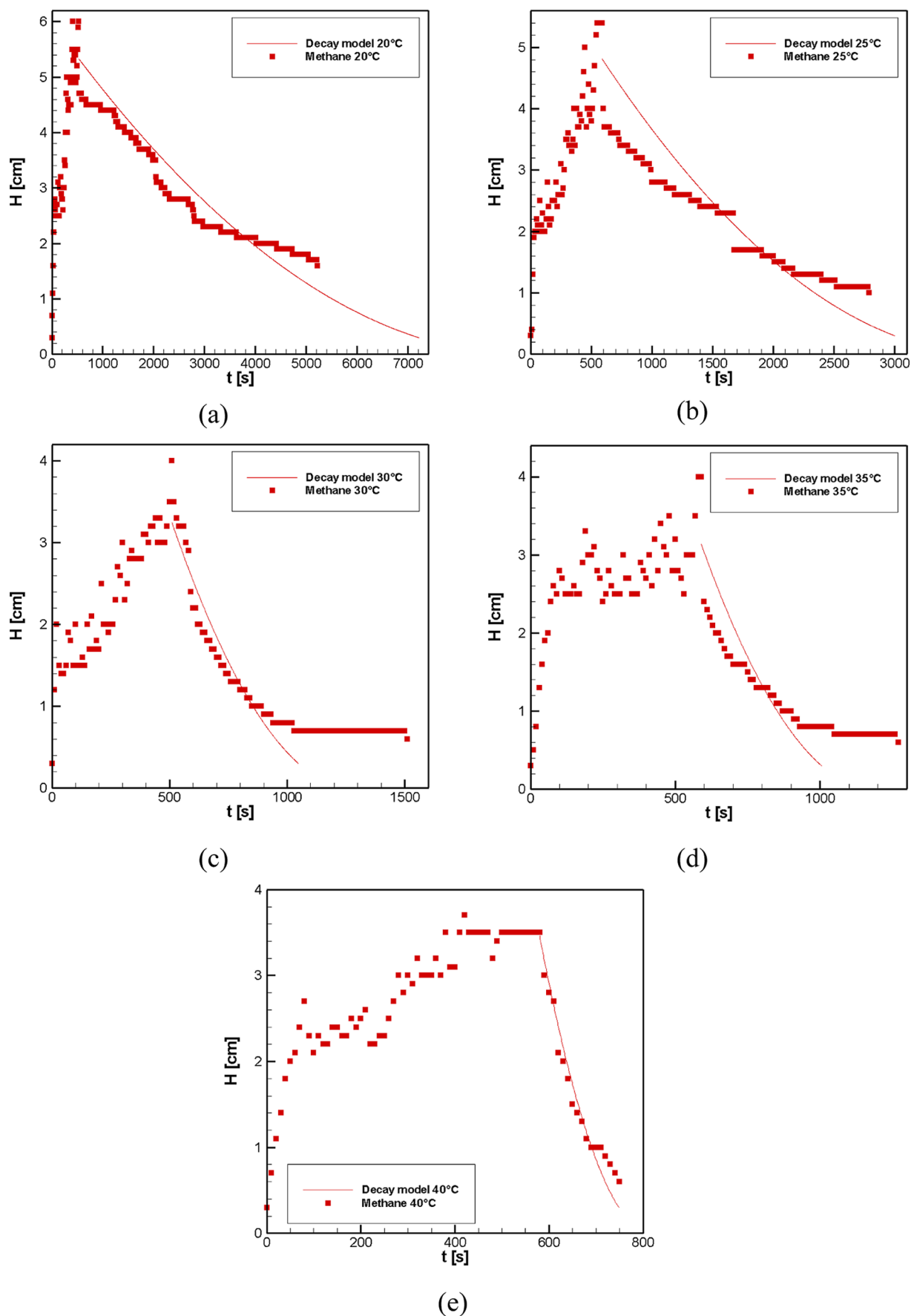


Figure 20. Decay mathematical modeling results for 1 bar methane. (a) $T = 20\text{ }^{\circ}\text{C}$, (b) $T = 25\text{ }^{\circ}\text{C}$, (c) $T = 30\text{ }^{\circ}\text{C}$, (d) $T = 35\text{ }^{\circ}\text{C}$, and (e) $T = 40\text{ }^{\circ}\text{C}$.

Table 6. C_3 Adjust and RMSE Results

	temperature [°C]	C_3	RMSE	normalized RMSE (%)
P1	20	3.40×10^{-6}	0.2731	4
P2	25	5.40×10^{-6}	0.3834	8
P3	30	1.01×10^{-5}	0.5351	9
P4	35	3.19×10^{-5}	0.4418	8
P5	40	2.85×10^{-5}	0.2355	7
P9	20	2.50×10^{-6}	0.3552	6
P10	25	6.50×10^{-6}	0.4849	10
P11	30	2.22×10^{-5}	0.2589	7
P12	35	2.80×10^{-5}	0.3885	11
P13	40	7.40×10^{-5}	0.1979	6
			average error	7

through mathematical modeling and coefficient adjustment are shown in Figures 19 and 20.

As can be seen, the decay model is similar, in its behavior, to the results obtained experimentally. It is also possible to observe that generally, the model predicts a more accelerated decay of the foam. This happens because in the inputs of the models, some simplifying hypotheses are used. In addition, the adjustment of the C_3 contributes to maintain a good correlation between the experimental results and the mathematical model. This nevertheless indicates that the model still lacks some corrections to become less dependent on this adjustment variable. From a graphical analysis of the results, as well as from the analysis related to the RMSE, it can be said that the results shown here are satisfactory.

4. CONCLUSIONS

The experimental results show that the temperature and pressure significantly affect foam formation and decay. Higher temperatures accelerate foam decay due to increased Ostwald ripening and decreased viscosity. Higher pressures increase foam stability by producing smaller bubbles, reducing Plateau borders, and slowing down Ostwald ripening. The type of gas injected also influences foam behavior, with gases of higher solubility causing an inversion of the decay curve. Two mathematical models were presented that require further development to improve accuracy. The foam formation model is limited by simplified assumptions, leading to linear curves instead of a more realistic steady state. The decay model depends heavily on empirical variables due to simplifying assumptions; therefore, a more complex model would improve results without the need for calibration. Overall, the study shows that despite differences in foam-forming fluids, foam behavior is comparable to the existing literature, allowing for direct comparison of results.

APPENDIX A

According to the hypotheses made previously in the Section 2.6, applying the conservation of mass in the gas phase inside of the control volume yields

$$\frac{dm_g(t)}{dt} = \rho_g j A \quad \text{if } t \leq \tau \quad (13)$$

where ρ_g is the gas phase density, j is the superficial gas velocity, A is the compartment cross-sectional area, m_g is the mass of gas in the system, and t is the time.

The total mass of gas trapped in the foam can also be written as a function of gas volume fraction as follows

$$m_g(t) = \int_0^{H(t)} \rho_g \phi(z, t) A dz \quad (14)$$

It is also known that the average gas volume fraction of the foam will be given by the following equation

$$\phi(t) = \frac{1}{H(t)} \int_0^{H(t)} \phi(z, t) dz \quad (15)$$

where $H(t)$ is the foam height as a function of time, $\bar{\phi}(t)$ is the average gas volume fraction of the foam and $\phi(z, t)$ is the gas volume fraction as a function of position and time, obtained through the correlation presented by Pilon et al.³²

Considering that the density of the gas is constant and the cross-sectional area also remains constant, (14) can be rewritten as follows

$$m_g(t) = \rho_g A \int_0^{H(t)} \phi(z, t) dz \quad (16)$$

Relocating the term of (15) one can write

$$\phi(t)H(t) = \int_0^{H(t)} \phi(z, t) dz \quad (17)$$

Substituting (17) into (16) the following expression is obtained

$$m_g(t) = \rho_g A \phi H(t) \quad (18)$$

Relocating the terms of (18) the following expression for the height of the foam layer is obtained as a function of time

$$H(t) = \frac{m_g(t)}{\rho_g A \bar{\phi}} \quad (19)$$

However, (13) can be integrated as follows

$$\int dm_g(t) = \int_0^t \rho_g j A dt \quad (20)$$

Then

$$m_g(t) = \rho_g j A t \quad (21)$$

Substituting (21) into (19)

$$H(t) = \frac{\rho_g j A t}{\rho_g A \bar{\phi}} \quad (22)$$


Simplifying

$$H(t) = \frac{j t}{\bar{\phi}} \quad (23)$$

It is possible to find the (1) showed in Section 2.6.

AUTHOR INFORMATION

Corresponding Author

Moisés A. Marcelino Neto — Multiphase Flow Research Center—NUEM, Federal University of Technology-Paraná (UTFPR), 80230-901 Curitiba, Paraná, Brazil;
 orcid.org/0000-0001-5492-6640; Email: mneto@utfpr.edu.br

Authors

Erich T. Tiunan — Multiphase Flow Research Center—
NUEM, Federal University of Technology-Paraná (UTFPR),
80230-901 Curitiba, Paraná, Brazil

Fabício S. da Silva — PETROBRAS—CENPES/PDIDP/
ESUP/TPMF, 21941-915 Rio de Janeiro, Rio de Janeiro,
Brazil

Rigoberto E. M. Morales — Multiphase Flow Research
Center—NUEM, Federal University of Technology-Paraná
(UTFPR), 80230-901 Curitiba, Paraná, Brazil;

orcid.org/0000-0003-3297-7361

Complete contact information is available at:

<https://pubs.acs.org/10.1021/acsomega.3c04565>

Author Contributions

Erich Tiunan: conceptualization, methodology, investigation, and writing—original draft. Moisés A. Marcelino Neto: conceptualization, methodology, investigation, and writing—review and editing. Fabício S. da Silva: conceptualization, methodology, investigation, and writing—review and editing. Rigoberto E. M. Morales: conceptualization, methodology, investigation, and writing—review and editing.

Notes

The authors declare no competing financial interest.

ACKNOWLEDGMENTS

The authors acknowledge the Leopoldo Americo Miguez de Mello Research and Development Center—CENPES/PETROBRAS for the financial support under the grant no. 5850.0106833.18.9.

REFERENCES

- (1) Wang, Z.; Li, S.; Peng, D.; Cheng, H.; Wei, Y. The Effect of Interfacial Tension on CO₂ Oil-Based Foam Stability under Different Temperatures and Pressures. *Fuel* **2023**, *341*, 127755.
- (2) Schramm, L. L. *Emulsions, Foams, and Suspensions*; Wiley, 2005.
- (3) Chen, J.; He, L.; Luo, X.; Zhang, C. Foaming of Crude Oil: Effect of Acidic Components and Saturation Gas. *Colloids Surf., A* **2018**, *553*, 432–438.
- (4) Sheng, F.; Zhang, J.; Yang, S.; Sun, G.; Li, C.; Yang, F.; Yao, B.; Jiang, X.; Zhou, Y. Foaming Characteristics of Crude Oil-CO₂Mixture by Depressurization: Influence of Crude Oil Viscosity and Wax Precipitation. *Colloids Surf., A* **2023**, *660*, 130887.
- (5) Zhang, Q.; Zuo, L.; Wu, C.; Sun, C.; Zhu, X. Effects of Crude Oil Characteristics on Foaming and Defoaming Behavior at Separator during CO₂ Flooding. *Colloids Surf., A* **2021**, *608*, 125562.
- (6) Shaban, H. I. A Study of Foaming and Carry-over Problems in Oil and Gas Separators. *Gas Sep. Purif.* **1995**, *9* (2), 81–86.
- (7) Monteiro, A. S.; da Silva, F. S. Multiphase Separator with Flushing System for Removing Accumulated Sand, and Method Using the Separator. AU 2018357084 A1, 2018. <https://lens.org/112-584-809-299-688>.
- (8) Poindexter, M. K.; Zaki, N. N.; Kilpatrick, P. K.; Marsh, S. C.; Emmons, D. H. Factors Contributing to Petroleum Foaming. 1. Crude Oil Systems. *Energy Fuels* **2002**, *16* (3), 700–710.
- (9) Zaki, N. N.; Poindexter, M. K.; Kilpatrick, P. K. Factors Contributing to Petroleum Foaming. 2. Synthetic Crude Oil Systems. *Energy Fuels* **2002**, *16* (3), 711–717.
- (10) Blázquez, C.; Dalmazzone, C.; Emond, E.; Schneider, S. Crude Oil Foams: Testing and Ranking of Antifoams with the Depressurization Test. *Energy Fuels* **2017**, *31* (2), 1285–1294.
- (11) Fink, J. *Petroleum Engineer's Guide to Oil Field Chemicals and Fluids*; Elsevier Science, 2012.
- (12) Fraga, A. K.; Santos, R. F.; Mansur, C. R. E. Evaluation of the Efficiency of Silicone Polyether Additives as Antifoams in Crude Oil. *J. Appl. Polym. Sci.* **2012**, *124* (5), 4149–4156.
- (13) Rezende, D. A.; Bittencourt, R. R.; Mansur, C. R. E. Evaluation of the Efficiency of Polyether-Based Antifoams for Crude Oil. *J. Pet. Sci. Eng.* **2011**, *76* (3–4), 172–177.
- (14) Abd Rahim, N. S.; Saaid, I. M.; Umar, A. A. Evaluation of Foam Performance at Different Temperature for Enhanced Oil Recovery Process. *World J. Eng.* **2019**, *16* (3), 412–418.
- (15) Buckingham, J. H. Effect of PH, Concentration, and Temperature on the Strength of Cytoplasmic Protein Foams. *J. Sci. Food Agric.* **1970**, *21* (9), 441–445.
- (16) Delahaije, R. J. B. M.; Lech, F. J.; Wierenga, P. A. Investigating the Effect of Temperature on the Formation and Stabilization of Ovalbumin Foams. *Food Hydrocolloids* **2019**, *91*, 263–274.
- (17) Fortkamp, F. P.; Barbosa, J. R., Jr. Refrigerant Desorption and Foaming in Mixtures of HFC-134a and HFO-1234yf and a Polyol Ester Lubricating Oil. *Int. J. Refrig.* **2015**, *53*, 69–79.
- (18) Holt, T.; Vassenden, F.; Svorstol, I. Effects of Pressure on Foam Stability; Implications for Foam Screening. *Proceedings—SPE Symposium on Improved Oil Recovery*; Society of Petroleum Engineers, 1996; Vol. 1, pp 543–552.
- (19) Indrawati, L.; Wang, Z.; Narsimhan, G.; Gonzalez, J. Effect of Processing Parameters on Foam Formation Using a Continuous System with a Mechanical Whipper. *J. Food Eng.* **2008**, *88* (1), 65–74.
- (20) Jackman, M.; Bussonnière, A.; Leung, H. L.; Xu, Z.; Tsai, P. A.; Liu, Q. Effect of Temperature on Foamability Using a Thermoresponsive Polymer. *AIP Adv.* **2018**, *8* (7), 075320.
- (21) Kamath, S.; Huppertz, T.; Houlihan, A. V.; Deeth, H. C. The Influence of Temperature on the Foaming of Milk. *Int. Dairy J.* **2008**, *18* (10–11), 994–1002.
- (22) Kapetas, L.; Vincent Bonniou, S.; Danelis, S.; Rossen, W. R.; Farajzadeh, R.; Eftekhari, A. A.; Mohd Shafian, S. R.; Kamarul Bahrim, R. Z. Effect of Temperature on Foam Flow in Porous Media. *J. Ind. Eng. Chem.* **2016**, *36*, 229–237.
- (23) Maini, B. B.; Ma, V. Laboratory Evaluation of Foaming Agents for High Temperature Applications—I. Measurements of Foam Stability At Elevated Temperatures and Pressures. *J. Can. Pet. Technol.* **1986**, *25* (06), 969–975.
- (24) Szabries, M.; Jaeger, P.; Amro, M. M. Foam Analysis at Elevated Pressures for Enhanced Oil Recovery Applications. *Energy Fuels* **2019**, *33* (5), 3743–3752.
- (25) Szabries, M.; Sergelius, S.; Kordts, A.; Jönsson, M. Foam Stability and Foam Structure under High Pressure for Tertiary Oil Production. *Appl. Rep.* **2019**, *1*.
- (26) Farajzadeh, R.; Vincent-Bonniou, S.; Bourada Bourada, N. Effect of Gas Permeability and Solubility on Foam. *J. Soft Matter* **2014**, *2014*, 1–7.
- (27) Gregorian, R.; Bafford, R.; Duke, M. Influence of Foaming Gas on Foam Stability. *Text. Res. J.* **1983**, *53* (5), 267–270.
- (28) Hartland, S.; Bourne, J. R.; Ramaswami, S. A Study of Disproportionation Effects in Semi-Batch Foams-II. Comparison between Experiment and Theory. *Chem. Eng. Sci.* **1993**, *48* (9), 1723–1733.
- (29) Hanamertani, A. S.; Saraji, S.; Piri, M. A Comparative Investigation of the Effect of Gas Type on Foam Strength and Flow Behavior in Tight Carbonates. *Chem. Eng. Sci.* **2023**, *276*, 118798.
- (30) Bikerman, J. J. The Unit of Foaminess. *Trans. Faraday Soc.* **1938**, *34*, 634–638.
- (31) Pilon, L.; Fedorov, A. G.; Viskanta, R. Steady-State Thickness of Liquid-Gas Foams. *J. Colloid Interface Sci.* **2001**, *242* (2), 425–436.
- (32) Pilon, L. G.; G Fedorov, A.; Viskanta, R. Analysis of Transient Thickness of Pneumatic Foams. *Chem. Eng. Sci.* **2002**, *57* (6), 977–990.
- (33) Sita Ram Sarma, D. S. H.; Pandit, J.; Khilar, K. C. Enhancement of Stability of Aqueous Foams by Addition of Water-Soluble Polymers—Measurements and Analysis. *J. Colloid Interface Sci.* **1988**, *124* (1), 339–348.
- (34) Narsimhan, G. A Model for Unsteady State Drainage of a Static Foam. *J. Food Eng.* **1991**, *14* (2), 139–165.

- (35) Dedhia, A. C.; Ambulgekar, P. V.; Pandit, A. B. Static Foam Destruction: Role of Ultrasound. *Ultrason. Sonochem.* **2004**, *11* (2), 67–75.
- (36) Hutzler, S.; Lösch, D.; Carey, E.; Weaire, D.; Hloucha, M.; Stubenrauch, C. Evaluation of a Steady-State Test of Foam Stability. *Philos. Mag.* **2011**, *91* (4), 537–552.
- (37) Mannhardt, K.; Novosad, J. J.; Schramm, L. L. Comparative Evaluation of Foam Stability to Oil. *SPE Reservoir Eval. Eng.* **2000**, *3* (01), 23–34.
- (38) Osama Al, A. B. Foamability and Foam Stability of Several Surfactants Solutions: The Role of Screening and Flooding. *J. Pet. Environ. Biotechnol.* **2015**, *06* (04), SPE-172185-MS.
- (39) Simjoo, M.; Rezaei, T.; Andrianov, A.; Zitha, P. L. J. Foam Stability in the Presence of Oil: Effect of Surfactant Concentration and Oil Type. *Colloids Surf., A* **2013**, *438*, 148–158.
- (40) Treter, J.; Peixoto, M. P. G.; Ortega, G. G.; Canto, G. S. Foam-Forming Properties of *Ilex Paraguariensis* (Mate) Saponin: Foamability and Foam Lifetime Analysis by Weibull Equation. *Quim. Nova* **2010**, *33* (7), 1440–1443.
- (41) Pilon, L.; Viskanta, R. Minimum Superficial Gas Velocity for Onset of Foaming. *Chem. Eng. Process.* **2004**, *43* (2), 149–160.
- (42) Wilson, A. J. *Foams: Physics, Chemistry and Structure*; Wilson, A., Ed.; Springer Series in Applied Biology; Springer London: London, 1989.
- (43) Kaviani, M. *Principles of Heat Transfer in Porous Media; Mechanical Engineering Series*; Springer New York: New York, NY, 1995; Vol. 53.
- (44) Farajzadeh, R.; Krastev, R.; Zitha, P. L. J. Gas Permeability of Foam Films Stabilized by an α -Olefin Sulfonate Surfactant. *Langmuir* **2009**, *25* (5), 2881–2886.
- (45) Cantat, I.; Cohen-Addad, S.; Elias, F.; Graner, F.; Höhler, R.; Pitois, O.; Rouyer, F.; Saint-Jalmes, A.; Flatman, R. *Foams*; Cox, S., Ed.; Oxford University Press, 2013.
- (46) Govindu, A.; Ahmed, R.; Shah, S.; Amani, M. Stability of Foams in Pipe and Annulus. *J. Pet. Sci. Eng.* **2019**, *180*, 594–604.